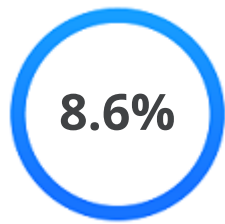




# QuillBot

## QuillBot

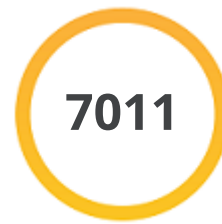
Scanned on: 6:39 December 15, 2022 UTC



Overall Similarity Score



Results Found











Total Words in Text

Identical Words	349
Words with Minor Changes	252
Omitted Words	0

## Results

Sources that matched your submitted document.

 <b>Electrochemical sensor based on screen printed carbon elec...</b> <a href="https://pubs.rsc.org/en/content/articlehtml/2022/ra/d1ra06862h">https://pubs.rsc.org/en/content/articlehtml/2022/ra/d1ra06862h</a>	2%
 <b>Electrochemical sensor based on screen printed carbon elec...</b> <a href="https://www.ncbi.nlm.nih.gov/pmc/articles/PMC8978621/">https://www.ncbi.nlm.nih.gov/pmc/articles/PMC8978621/</a>	1%
 <b>art-template-1.9.docx</b> <a href="https://www.rsc.org/globalassets/05-journals-books-databases/journal-au...">https://www.rsc.org/globalassets/05-journals-books-databases/journal-au...</a> art-template-1.9.docx	1%
 <b>icm-research-article-guideline-template.docx</b> <a href="https://www.rsc.org/globalassets/05-journals-books-databases/our-journa...">https://www.rsc.org/globalassets/05-journals-books-databases/our-journa...</a> icm-research-article-guideline-template.docx	1%
 <b>com-template-1.6.docx</b> <a href="https://www.rsc.org/globalassets/05-journals-books-databases/journal-au...">https://www.rsc.org/globalassets/05-journals-books-databases/journal-au...</a> com-template-1.6.docx	1%
 <b>com-template-1.8.docx</b> <a href="https://www.rsc.org/globalassets/05-journals-books-databases/journal-au...">https://www.rsc.org/globalassets/05-journals-books-databases/journal-au...</a> com-template-1.8.docx	1%
 <b>art-template-2.0.docx</b> <a href="https://www.rsc.org/globalassets/05-journals-books-databases/journal-au...">https://www.rsc.org/globalassets/05-journals-books-databases/journal-au...</a> art-template-2.0.docx	1%
 <b>Thermal decomposition and reconstitution of hydroxyapati...</b> <a href="https://9lib.co/document/ky6467gq-thermal-decomposition-reconstitution...">https://9lib.co/document/ky6467gq-thermal-decomposition-reconstitution...</a> ky6467gq-thermal-decomposition-reconstitution-hydroxyapatite-air-a...	1%

### IDENTICAL

Identical matches are one to one exact wording in the text.









### MINOR CHANGES









Nearly identical with different form, ie "slow" becomes "slowly".









Unsure about your report?

The results have been found after comparing your submitted text to online sources, open databases and the Copyleaks internal database. For any questions about the report contact us on [support@copyleaks.com](mailto:support@copyleaks.com)

[Learn more about different kinds of plagiarism here](#)

 <b>c7ay00588a1.pdf</b> <a href="http://www.rsc.org/suppdata/c7/ay/c7ay00588a/c7ay00588a1.pdf">http://www.rsc.org/suppdata/c7/ay/c7ay00588a/c7ay00588a1.pdf</a> c7ay00588a1.pdf	1%
 <b>Simultaneous and sensitive determination of ascorbic acid, ...</b> <a href="https://www.ncbi.nlm.nih.gov/pmc/articles/PMC7419206/">https://www.ncbi.nlm.nih.gov/pmc/articles/PMC7419206/</a>	1%
 <b>Simultaneous and sensitive determination of ascorbic acid, ...</b> <a href="https://jnanobiotechnology.biomedcentral.com/articles/10.1186/s12951-0...">https://jnanobiotechnology.biomedcentral.com/articles/10.1186/s12951-0...</a>	1%
 <b>Highly selective electrochemical sensing based on electropo...</b> <a href="https://pubs.rsc.org/en/content/articlehtml/2022/ra/d2ra05196f">https://pubs.rsc.org/en/content/articlehtml/2022/ra/d2ra05196f</a>	1%
 <b>Electrochemical sensor based on screen printed carbon elec...</b> <a href="https://pubs.rsc.org/en/content/articlepdf/2022/ra/d1ra06862h">https://pubs.rsc.org/en/content/articlepdf/2022/ra/d1ra06862h</a>	1%
 <b>Electrochemical-Based Biosensors on Different Zinc Oxide N...</b> <a href="https://www.ncbi.nlm.nih.gov/pmc/articles/PMC6766311/">https://www.ncbi.nlm.nih.gov/pmc/articles/PMC6766311/</a>	1%
 <b>c8mo00139a1.pdf</b> <a href="http://www.rsc.org/suppdata/c8/mo/c8mo00139a/c8mo00139a1.pdf">http://www.rsc.org/suppdata/c8/mo/c8mo00139a/c8mo00139a1.pdf</a> c8mo00139a1.pdf	1%
 <b>A new electrochemical sensor for simultaneous determinati...</b> <a href="https://pubmed.ncbi.nlm.nih.gov/31277046/">https://pubmed.ncbi.nlm.nih.gov/31277046/</a>	1%

 <b>Highly selective electrochemical sensing based on electropo...</b> <a href="https://www.ncbi.nlm.nih.gov/pmc/articles/PMC9574646/">https://www.ncbi.nlm.nih.gov/pmc/articles/PMC9574646/</a>	1%
 <b>c6ra12065b1.pdf</b> <a href="http://www.rsc.org/suppdata/c6/ra/c6ra12065b/c6ra12065b1.pdf">http://www.rsc.org/suppdata/c6/ra/c6ra12065b/c6ra12065b1.pdf</a> c6ra12065b1.pdf	1%
 <b>Electrochemical sensor for simultaneous determination of ...</b> <a href="https://www.sciencegate.app/document/10.1016/j.snb.2010.07.044">https://www.sciencegate.app/document/10.1016/j.snb.2010.07.044</a> j.snb.2010.07.044	1%
 <b>198099503.pdf</b> <a href="https://core.ac.uk/download/pdf/198099503.pdf">https://core.ac.uk/download/pdf/198099503.pdf</a> 198099503.pdf	1%
 <b>Hydroxyapatite coatings: a critical review on electrodeposit...</b> <a href="https://pubs.rsc.org/th-th/content/articlehtml/2022/ma/d2ma00620k">https://pubs.rsc.org/th-th/content/articlehtml/2022/ma/d2ma00620k</a>	1%
 <b>c4tb00764f1.pdf</b> <a href="http://www.rsc.org/suppdata/tb/c4/c4tb00764f/c4tb00764f1.pdf">http://www.rsc.org/suppdata/tb/c4/c4tb00764f/c4tb00764f1.pdf</a> c4tb00764f1.pdf	1%
 <b>C4CC08174A</b> <a href="https://pubs.rsc.org/en/content/getauthorversionpdf/C4CC08174A">https://pubs.rsc.org/en/content/getauthorversionpdf/C4CC08174A</a>	1%
 <b>RSC Article Template (Version 3.0)</b> <a href="http://wrap.warwick.ac.uk/40372/1/WRAP_Wills__OB-ART-06-2011-006010...">http://wrap.warwick.ac.uk/40372/1/WRAP_Wills__OB-ART-06-2011-006010...</a> WRAP_Wills__OB-ART-06-2011-006010_resubmission_aug_2011_%282...	1%

 <b>Simultaneous electrochemical sensing of ascorbic acid, dop...</b> <a href="https://pubmed.ncbi.nlm.nih.gov/22405300/">https://pubmed.ncbi.nlm.nih.gov/22405300/</a>	1%
 <b>Simultaneous electrochemical sensing of ascorbic acid, dop...</b> <a href="https://www.semanticscholar.org/paper/Simultaneous-electrochemical-se...">https://www.semanticscholar.org/paper/Simultaneous-electrochemical-se...</a>	1%
 <b>d0cp01087a1.pdf</b> <a href="http://www.rsc.org/suppdata/d0/cp/d0cp01087a/d0cp01087a1.pdf">http://www.rsc.org/suppdata/d0/cp/d0cp01087a/d0cp01087a1.pdf</a> d0cp01087a1.pdf	1%
 <b>Microsoft Word - ESI-PCCP-PKU Zou.docx</b> <a href="http://www.rsc.org/suppdata/cp/c1/c1cp22613d/c1cp22613d.pdf">http://www.rsc.org/suppdata/cp/c1/c1cp22613d/c1cp22613d.pdf</a> c1cp22613d.pdf	1%
 <b>EDTA assisted synthesis of hydroxyapatite nanoparticles for...</b> <a href="https://pubmed.ncbi.nlm.nih.gov/25063159/">https://pubmed.ncbi.nlm.nih.gov/25063159/</a>	1%
 <b>art07.pdf</b> <a href="https://www.scielo.cl/pdf/jcchems/v61n4/art07.pdf">https://www.scielo.cl/pdf/jcchems/v61n4/art07.pdf</a> art07.pdf	1%
 <b>STRUCTURE AND THERMAL BEHAVIOR OF TANNINS FROM Ac...</b> <a href="https://www.scielo.cl/scielo.php?pid=S0717-97072016000400007&amp;script=s...">https://www.scielo.cl/scielo.php?pid=S0717-97072016000400007&amp;script=s...</a> scielo.php	1%
 <b>Materials   Free Full-Text   Electrochemical-Based Biosensor...</b> <a href="https://www.mdpi.com/1996-1944/12/18/2985/htm">https://www.mdpi.com/1996-1944/12/18/2985/htm</a>	1%



**Materials | Free Full-Text | Electrochemical-Based Biosensor...**  
<https://www.mdpi.com/1996-1944/12/18/2985>

1%

Received 00th January 20xx,  
Accepted 00th January 20xx

DOI: 10.1039/x0xx00000x

www.rsc.org/

## A novel non-enzymatic electrochemical uric acid sensing based on extracted hydroxyapatite from eggshell biowaste on zinc oxide nanoparticles decorated activated carbon electrode (Hap-Esb/ZnONPs/ACE).

Retno Wulandari,<sup>ab\*</sup> Ardi Ardiansyah,<sup>a</sup> Henry Setiyanto<sup>d</sup>, and Vienna Saraswaty<sup>ac\*</sup>

A sensitive and selective electrochemical sensor, based on green synthesized hydroxyapatite from eggshell biowaste (Hap-Esb) was fabricated by a simple immobilization on zinc oxide nanoparticles decorated activated carbon paste electrode, was developed for detection of uric acid. Due to electrochemical oxidation of UA depending on the pH values, the sensor performance was tested at various pH values. The proposed sensor was thoroughly characterized by scanning electron microscopy, x-ray diffraction, and cyclic voltammetry. Excellent results were obtained for detection of UA in a linear range of 0.001–10  $\mu\text{M}$ . A limit of detection value of 0.016  $\mu\text{M}$  was calculated. The developed sensor showed an excellent selectivity towards some interferences that are ascorbic acid, glucose, and tyrosine. In addition, the sensor also showed a good repeatability for 16 times simultaneous UA evaluation with RSD value of 1.5%. Our work highlights that Hap-Esb can be used as a component of biosensor, and our proposed sensor is promising for a fast monitoring of UA level.

**Keywords:** Uric acid; Activated carbon electrode; Hydroxyapatite; electrochemical; eggshell

### Introduction

In the current field of disease diagnosis and treatment, there is a necessity to create a device that can identify, trace, and quantify metabolites of several important biochemical processes of human body for a fast, straightforward, and accurate diagnosis of variety disorder. Uric acid (UA), a natural antioxidant and byproduct of purine metabolism, and its derivatives are required for biological activity in the human body [1] and [2]. The excess UA concentration from its typical range is linked with several disease such as gout, cardiovascular [3], hyperuricemia [4], and type II diabetes [5].

Meanwhile a lower amount of UA than its typical range may reflect to an earlier stage of Parkinson, Alzheimer, as well as Multiple sclerosis disease [6] and [7]. Therefore, a device that can monitor UA is become important.

Several analysis methods including high performance liquid chromatography, chemiluminescence analysis, spectrophotometry, and electrochemical analysis have been used for routine UA analysis. Among them, electrochemical analysis has received more attention because of its fast, reliable, and accurate result. More importantly, by applying an electrochemical analysis, the small quantity of an electroactive element can be detected accurately.

To date, most of routine UA sensing applies an enzymatic electrode. By applying an enzymatic electrode, the presence of UA can be detected accurately due to its selectivity. However, an enzymatic sensing has several limitations that are must be placed at low temperature, has a short lifetime, and must be packed properly. Several reports have proposed applying hydroxyapatite (Hap) in decorating electrode surface for detection of UA. This is reasonable because the interaction between urate ions (Lewis bases) with Lewis acid sites due to the presence of  $\text{Ca}^{2+}$  ions from the Hap lattice causes the acidity of the Hap surface resulting in an increase in the interaction of redox pairs [8] [9] [10] [11] [12] and

<sup>a</sup> Research Center for Environmental and Clean Technology, National Research and Innovation Agency Republic of Indonesia, Bandung, Indonesia.

<sup>b</sup> Chemical Engineering Department, Faculty of Engineering, Universitas Bhayangkara Jakarta Raya, Jl. Harsono RM no.67, Jakarta.  
e-mail: Retno.wulandari@ubharajaya.ac.id

<sup>c</sup> Collaborative Research Center for Sustainable and Zero Wastes Industries, Universitas Kristen Wiyata Mandala Surabaya,  
e-mail: vien001@brin.go.id.

\* Footnotes relating to the title and/or authors should appear here.

Electronic Supplementary Information (ESI) available: [details of any supplementary information available should be included here]. See

[13]. Hap surface acidity becomes the dominant influencing factor [14] and [15]. In addition, Hap modified electrodes have been extensively studied due to their acid-base properties, ion-exchange capabilities, and high adsorption capacities [16] [17] and [18]. Thus, the development of non-enzymatic UA sensing based Hap is of interest.

Hap can be synthesized by various technique including precipitation, hydrolysis, hydrothermal synthesis and/or extracted from natural resources, for example seashells, shrimp shells, bovine bones, fish bones. It is very important to note that food-industries generally use eggs in the production of cakes, foods, and so on [19]. The high demand of eggs in food production making the amount of eggshell biowastes (Esb) are available abundantly. An eggshell is structurally composed of three layers that are cuticle, spongy layer and the lamellar layer. The spongy and lamellar layers resemble a matrix of protein fibers tied to the calcium carbonate (calcite) crystal at a ratio of 1:50. The content of calcite in eggshell is about ~94%, making eggshell is very potential for being valorized become Hap [20] [21]. A study reported that Hap can be extracted from eggshell by a simple two stage thermal treatment at 450° and 1000°C in a furnace. For this reason, we develop a UA sensing based on extracted Hap from Esb. By utilizing the Esb for the extraction of Hap, we, therefore, play a role in the environmental sustainability as well as waste management [22]. More importantly, this will also increase the added value of Esb.

The performance of UA Hap based sensor is influenced by the surface acidity of Hap and mesopore volume. In addition, high agglomeration with decreased proportion of discrete Hap particles was found to decrease the electrochemical active sites [23] and [24]. Therefore, decorating the developed Hap based electrode for a better current response is required.

Zinc oxide (ZnO) has recognized as a promising biosensor material because of its unique features. The following is a summary list of ZnO features that enables it useful for wide biosensor applications includes: direct and wide band gap, large exciton binding energy, large piezoelectric constant, strong luminescence, strong sensitivity of surface conductivity to the presence of adsorbed species, strong non-linear resistance of polycrystalline ZnO, large non-linear coefficients, high thermal conductivity, available of large single crystal, as well as amenability to wet chemical etching [25] [26] [27] [28] [29] [30] and [31]. In addition, the high isoelectric point of ZnO enables to improve the absorption [32] [33][34] and [35]. Zinc oxide has the ability to enhance electron transport and enhance catalytic processes [36] [37]. The ZnO nanoparticles used in this study are zero-dimensional in brief, 0-D ZnO is a basic elemental unit consisting of nanoparticles [38] and collection points [39], thus requiring modifications to enhance the electron immobilization capability. The HAP coating can provide a good surface for immobilizing nanostructured materials on the electrode surface because it is easy to function and also creates conditions to facilitate the process of electron transfer through a synergistic action between itself and the mediator [40] and [41]. We therefore decorated a UA sensing based Hap developed with ZnO to facilitate better electron transfer then improve the current sensor response. We therefore decorated the developed UA sensing based

Hap with ZnO to facilitate a better electron transfer then improving the current sensor's response.

In this present investigation, we reported a novel non-enzymatic UA electrochemical sensing based extracted Hap from Esb on activated carbon electrode (ACE) surface. The Hap with improved activity was immobilized on ZnO nanoparticles decorated on the ACE surface. The electrochemical characteristics and response behavior of developed electrode was evaluated by cyclic voltammetry (CV). The analytical performance of the developed electrode toward UA analysis was also demonstrated.

## Experimental Section

### Materials and Instruments

Eggshell biowastes were collected from the disposal of the foods located in Bandung City, Indonesia. Activated carbon,  $\text{Zn}(\text{CH}_3\text{COOH})_2 \cdot 2\text{H}_2\text{O}$  (99.5–101.0%),  $\text{KH}_2\text{PO}_4$  ( $\geq 99.995\%$ ), and  $\text{K}_2\text{HPO}_4$  ( $\geq 99.99\%$ ) are from Merck (Germany) with pro analytical grade. Ultrapure water was prepared by a Module E-pure D4642-33 instrument (Farnstead) with a resistivity  $\geq 18 \text{ M}\Omega$ .

Particle size analysis was performed using a Zetasizer Nano Series, Malvern (UK). An UV-visible spectrophotometer (Agilent Technologies-8453, Germany) was used to quantify absorbance. The surface morphology of the extracted Hap and synthesized ZnONPs was examined using scanning electron microscopy (SEM; JEOL JSM IT300, Japan). Comparatively, an EDX (Oxford X-Max 20, UK) evaluation was used to determine the element that was present on the electrode surface. The Autolab PGSTAT302N Metrohm was used to record the electrochemical measurement. A three-electrode system was used with Ag/AgCl reference and Pt counter electrodes. The working electrode was ACE modified with ZnONPs and HAP.

### Synthesis and Characterization of ZnO NPs

The ZnONPs were synthesized following the previous work [1]. In separated flasks, about 200 mL of 0.1 M of  $\text{Zn}(\text{CH}_3\text{COOH})_2 \cdot 2\text{H}_2\text{O}$  and 200 mL of 0.4 M KOH were dissolved in ethanol. Until completely dissolved, both solutions were heated at 60°C while being constantly stirred. The KOH solution was then gradually added to the  $\text{Zn}(\text{CH}_3\text{COOH})_2 \cdot 2\text{H}_2\text{O}$  solution and agitated continuously for 3 hours. The white precipitate that contained the zinc oxide particles was produced. Centrifugation was then used to separate the ZnO particles at a speed of 4000 rpm. The contaminants were then removed from the ZnO particles using acetone and ultrapure water before being heated at 600 C to create ZnONPs (2.2 grams).

### Extraction, synthesis, and characterization of Hap-Esb

The Esb were rinsed with tap water and dried under sun before grounded. The dried Esb were then grounded by using a grinder machine and sieved with a 100 mesh sieve size. The CaO was extracted from Esb by calcination in a furnace at temperature of 1000°C for 5 h. Next, the extracted CaO from Esb was further transformed become Hap by stirring the extracted CaO in 0.6M  $\text{H}_3\text{PO}_4$  solution at ratio of 1:1 The mixture was heated at 60 °C.



Prior to heating process, the mixture was sonicated (40 kHz, 1 h) for homogenization as well as to redisperse the CaO aggregation by using a ultrasonic instrument (Merk, Negara). The process was carried out for 24 h incubation. Next, the synthesized Hap was separated from the filtrate by centrifugation (3000 rpm, 15 min).

The precipitate was then dried in an oven at 105 C for overnight.

Finally the precipitate was heated in a furnace (1000 C, 5h) with the heating rate of 600 °C/h for a complete transformation of CaO become Hap. The synthesized Hap-Esb was then characterized by SEM, X-ray diffraction, and XRF.

### Decoration of ZnONPs on ACE surface (ZnO/ACE)

The following steps are used to create the modified active carbon electrode: First, 0.5 g of active carbon electrode powder was added 100 µL of paraffin oil as a binder. The mixture was then combined for 30 min in a small mortar. Second, 10% ZnONPs made from purified ZnO nanopowders. The hole in the electrode body was filled with the produced paste (mixture of active carbon with paraffin). The electrode body, which is in contact with a copper wire, is a capillary pipe with a hole at one end (with an inner diameter of 2.0 mm) for the carbon paste filling. then, ZnONPs is inserted into the capillary tube hole. A copper wire inserted into the opposite end of the tube made electrical contact. The ZnONPs/ACE surface was polished with weighing paper when the electrode surface needed to be renewed.

### Modification of ZnONPs/ACE electrodes with HAp

Modification performed by adding 10% HAp from of massa ZnONPs/ACE. The hole in the electrode body has been filled with the result of the above method added HAp in a way is inserted into the capillary tube hole. The HAp/ZnONPs/ACE surface was polished with weighing paper when the electrode surface needed to be renewed.

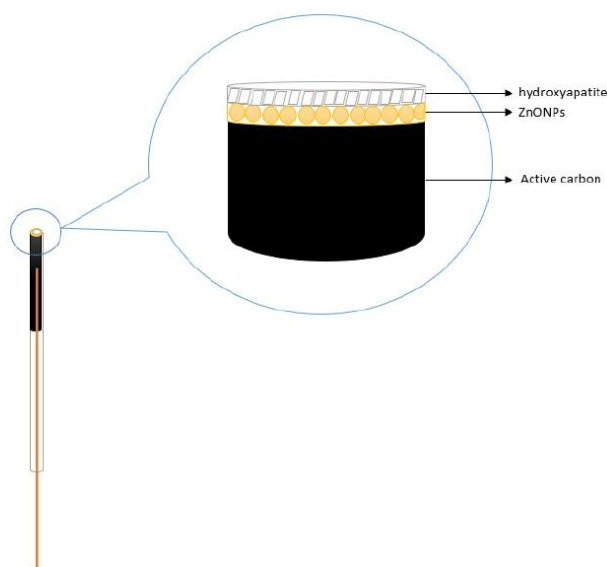


Fig. 1 Schematic representation of the Hap-Esb/ZnONPs/ACE

### Electrochemical measurements

Using a potentiostat that was operated by a computer, electrochemical measurements were made (Metrohm, Autolab). A typical three-electrode cell with a 20 mL capacity was employed. In 20 mL of 0.1 M PfiS pH 8, the potential window measurement was performed. A Pt counter electrode (CE) with a diameter of 0.5 mm (fio-Logic Science Instruments, A-002222) and an Ag/AgCl reference electrode (RE) with a diameter of 2 mm (World Precision Instruments, DRIRFE-2) for the electrochemical studies. The working electrode was a HAp/ZnONPs/ACE. ZnO and HAp nanocoats were

added to the surface respectively using 10% of the carbon paste by weight used. Cyclic voltammetry was used for electrochemical measurements of uric acid (UA) standard solutions and samples on ZnONPs/ACE modified by HAp (HAp/ZnONPs/ACE) electrodes from the potentials of  $-1.5$  V to  $1.8$  V at a scan rate of 100 mV/s. The standard solutions were prepared in Phosphate buffer solution (PfiS) pH 8 with various concentrations of UA (0.001 - 10) µM. This step is carried out to determine the working range of the sensor in detecting UA. Measurements were also carried out in the presence of interfering compounds such as ascorbic acid, glucose and tyrosine to find out whether the modified sensor uses selective HAp in UA measurement. The simplified electrochemical measurements setup used in this study are shown in Figure 2.

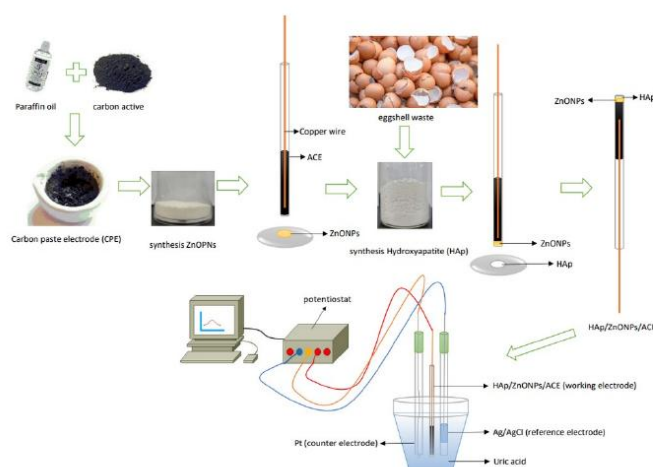


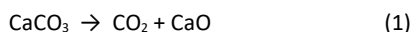
Fig. 2 Schematic Electrochemical measurements uric acid using the Hap-Esb/ZnONPs/ACE

## Results and discussion

### Characterization of Hap-Esb

The extraction of CaO from Esb was performed by calcined the Esb at 1000 C for 5 h. In this step the calcite from eggshell will be transformed become CaO in accordance with the reaction Eq. 1. The presence of spongy and lamellar matrix that are not thermally

stable and tied with the calcite from eggshell will be decomposed and eliminated [42] [43].



Next, the synthesis of Hap-Esb was performed by mixing the Hap with  $\text{H}_3\text{PO}_4$  solution, followed by two heating stage. At the first heating stage, the temperature was set at 105 C for overnight (approximately 16 h). The main objective of the first heating stage is to remove water as well as moisture, while the second stage is critical for the formation of Hap. The surface morphology of synthesized Hap-Esb is presented in Fig. 3, as depicted at 5000x magnification, the synthesized Hap-Esb were found in the mixture of coral shapes constructed with hexagonal rods, and square-tile like shapes [44] [45]. When the magnification was adjusted to 30.000x, the mixture of particles at sub-micron and nano size were found as suggested by red and yellow circles. It seems the larger particle (sub-micron size) are formed from agglomeration. It is not surprising, because during synthesis of Hap, we applied two stage heating process, in which the second stage utilizing very high temperature for 5 h, then possibly to Hap particles are partly melted and may form a range of calcium phosphates including calcium oxide (CaO) or amorphous calcium phosphate upon decomposition [46] [47]. When the high-temperature particles are impacted onto the cold metal substrate (usually below 150 °C), the cooling rate of coatings can lead to the formation of crystalline, non-crystalline and metastable crystalline products such as oxyhydroxyapatite,  $\alpha$ -tricalcium phosphate, tetracalcium phosphate, calcium oxide (CaO) and amorphous apatite in HAP coatings [21] [48].

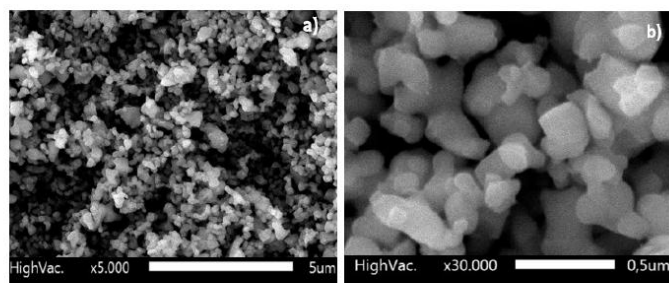


Fig. 3 SEM of Hap synthesis from eggshell

Next, the purity of Hap-Esb was further characterized by X-ray fluorescence (XRF). As tabulated in Table 1, the Hap-Esb contains Ca, Fe, Sr, Mn, and Sc elements. As expected, the Ca content were found at 99% concentration. So that the impurities present in eggshell did not interfere the transformation of CaO to become Hap.

Table 1. Element analysis XRF of Eggshells material (CaO)

element	Ca	S	Fe	Sr	Mn	Sc	Zn
percentag e	99.6 5	0.0 0	0.0 5	0.1 1	0.0 5	0.12 6	0.0 0

X-ray diffraction (XRD) analysis was used to characterize the Hap-Esb and compare the obtained XRD pattern to the database of the Joint Committee on Powder Diffraction Standards (JCPDS Card) [49]. As presented in Fig. 4b, the XRD pattern of Hap-Esb clearly showed peaks at  $2\theta$  values of 10.84, 16.99, 21.85, 22.84, 25.84, 27.82, 28.91, 31.75, 32.16, 32.88, 34.03, 35.59, 38.53, 40.41, 41.96, 46.80, 49.44, 49.58, and 52.05 which matched to the crystallographic planes (100), (101), (200), (111), (002), (102), (210), (211), (112), (300), (202), (301), (220), (310), (131), (113), (222), (213), and (322) respectively. This is in agreement with the HAP standard (JCPDS card no. 9-432) [50] (see Fig. 4a).

The crystallite sizes of Hap-Esb were then calculated using the Debye Scherer formula,

$$D = (0.89\lambda) / (\beta \cos\theta)$$

D denotes for the size of the crystallite, the full width at half maximum, the diffraction angle (theta), and the XRD wavelength. The crystallite sizes of Hap-Esb were tabulated in Table 2. The average Hap-Esb crystallite sizes was about 78.97 nm. In contrary with larger particles appeared in the SEM images, the calculated crystallite size emphasized the formation of aggregates of Hap-Esb.

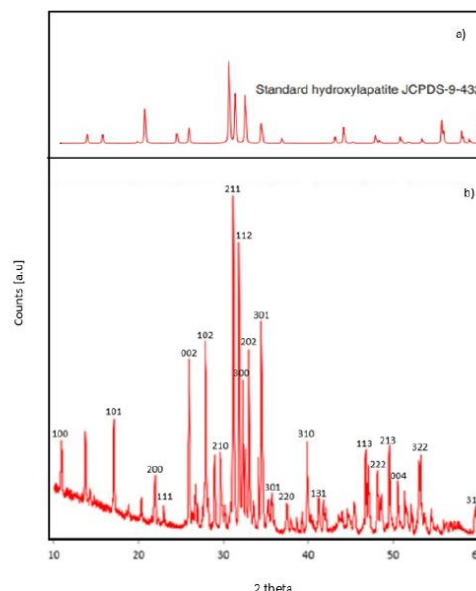


Fig4. XRD pattern of a) Hap (JCPDS Card No. 9-432) b) products Hap from eggshell obtained by precipitation method

Table 2. Calculation of crystallite size of Hap from eggshell

2 theta position	Crystallite size (nm)
10,84	48.89
16,99	65.65
21,85	66.12
22,84	99.31
25,84	66.61

## PCCP

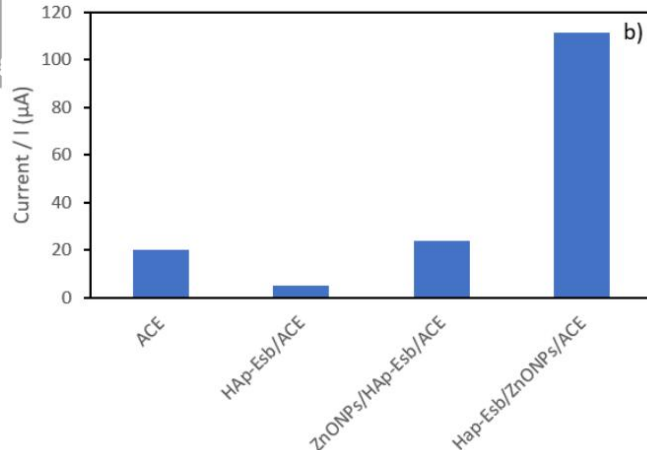
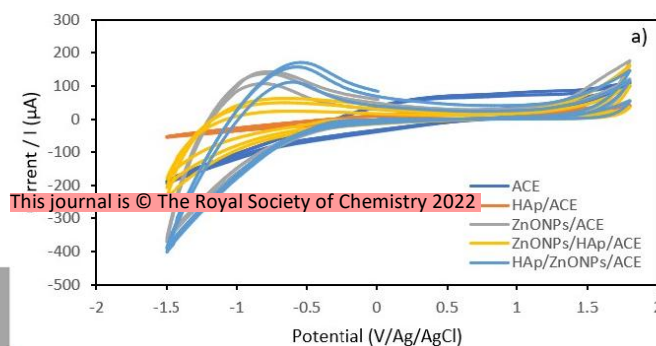
2 theta position	Crystallite size (nm)
27,82	100.29
28,91	67.05
31,75	67.50
32,16	101.31
32,88	101.50
34.03	101.80
35.59	51.12
38.53	103.12
40.41	103.73
41.96	52.13
46.80	70.74
49.44	107.17
49.58	53.61
52.05	72.75
Average	78.97

### Characterization of synthesis Zinc Oxide Nanoparticles (ZnONPs)

The wet chemical approach of synthesizing ZnO resulted in nano-sized particles, according to the particle size analysis (PSA) results. According to Fig., the particle size distribution of ZnONPs revealed a monodisperse system with a polydispersity index (PI) of 0.168 and an average diameter size of 71 nm [17]. ZnONPs were found to have a maximum absorption peak at = 377 nm (Fig.), which indicates that they were in the form of hexagonal wurtzite. The production of nanoparticles of the produced ZnONPs was highlighted in the SEM image (Fig.). The SEM image clearly demonstrates that the produced ZnONPs are crystalline, have a wurtzite structure, and have particles smaller than 100 nm, as shown. The findings of the evaluation of particle size and maximum absorption peak [51], [52], [53], [54], and [55] are strongly related to this. (nantini terakhir saja)

### Cyclic voltammetry (CV) behavior of the modified electrode toward UA response

CV technique was applied to evaluate the electrochemical behavior of the modified electrode toward 100 nM UA response in 0.1M PfiS solution at pH 8 at a potential range of -1.5 to 1.8 V and a scan rate of 100 mVs<sup>-1</sup>. The CV voltammogram for 100 nM UA on the bare ACE, Hap-Esb/ACE, ZnONPs/ACE, Hap-Esb/ZnONPs/ACE, ZnONPs/Hap-Esb/ACE are presented in Fig. 3a. There were a good response in the peak at -0.53 V corresponding to UA electro-oxidation. We also revealed that the greatest peak current response was observed on the Hap-Esb/ZnONPs/ACE (111.48 μA) surface in comparison with the bare ACE (30.6 μA), Hap-Esb/ACE (8.10 μA), and ZnONPs/Hap-Esb/ACE (24.02 μA)) (See Fig. 3b), indicating the enhanced sensitivity of the developed electrode towards UA electro-



oxidation. It is very imperative to note that the layer arrangement on modification of electrode surface is critical towards currents response[56]. When the ZnO NPs layer was bring forward on the outermost surface of developed sensor (ZnONPs/Hap-Esb/ACE), the ZnO particles blocked the Hap-Esb pore then reducing the current response. In reverse, when the ZnO NPs was send backward between Hap-Esb and ACE (Hap-Esb/ZnONPs/ACE), the current response elevated significantly 3 times higher than the bare ACE as well as the ZnONPs/Hap-Esb/ACE. Factors that affect the electrochemical response are (1) analyte diffusion, (2) catalyst, and (3) electron transfer [57]. fiy placing the Hap at the outermost surface, this improve the diffusion of UA, and the presence of ZnO NPs in the middle layer facilitating a better electron transfer, remarkably resulting in the highest current response.

Fig. 3 a). The CV voltammogram and b). Histogram of ACE modification oxidation peak

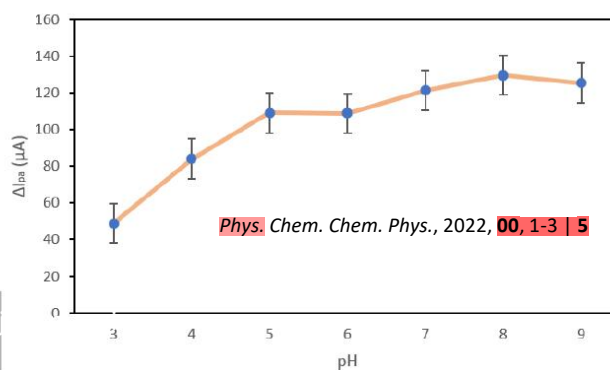
### Optimization of Hap/ZnONPs/ACE

**The influence of pH.** The effect of pH on the peak current response of UA has been observed at the Hap-Esb/ZnONPs/ACE in 0.1M PfiS over the pH range 3 to 9. CVs recorded in the presence of 0.1 μM UA at the scan rate of 100 mVs<sup>-1</sup> are shown in Fig. X. The results show that the UA peak current response increased gradually at pH 3 to 8, and starting to decrease at pH 9. In electro-analytical evaluation, the pH of solution significantly influence the current response since the protons are involved in the reaction [14]. It is known that Ca<sup>2+</sup> ions are present on the Hap-Esb, suggesting that the Ca<sup>2+</sup> ions take part in electrode reactions [58] [59] [58] and [60]. The maximum oxidation UA current was obtained at pH 8, hence this value was selected for further evaluation.

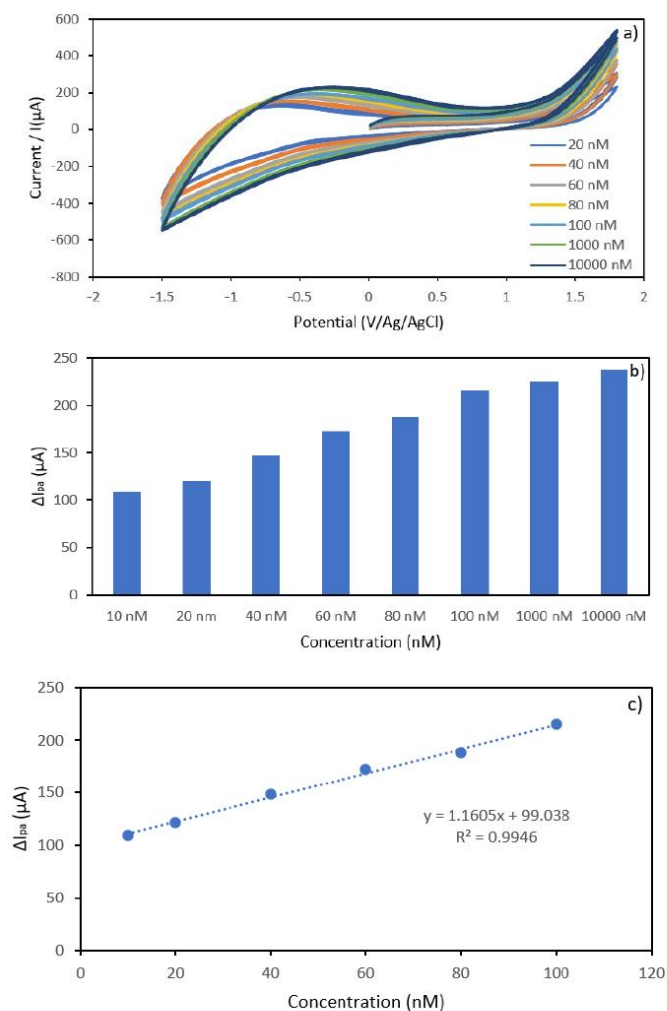
Fig. 4 pH on anodic current of 100 nM UA on the Hap-Esb/ZnONPs/ACE.

### Calibration plot and limit of detection benerin dulu hitungan LOD dan LOQ nya.

A calibration plot was constructed to assist quantitative retrieval of UA in real samples using the most proficient electrodes Hap-Esb/ZnONPs/ACE. Figure 5 presents the CV voltammograms



recorded using HAp/ZnONPs/ACE at various concentrations of UA, from 0.001–10  $\mu\text{M}$ , in a 0.1 M phosphate buffer at pH 8.0. It can be concluded from the inset of Figure 5, that the current response ( $I_p$ ) increases linearly with the concentration of UA in that range, with the linear regression equation  $I_p (\mu\text{A}) = 1.1605x + 99.038$  having a good correlation coefficient of 0.9946. The detection limit (based on 3 $\sigma$ ) is estimated to be 15,79 nM. The linear current response and limit detection obtained in this study are compared with the literature and presented in Table 3 to determine their competence



with other UA sensors. It can be noted from Table 3, that the proposed UA sensor is superior to those available in the literature, in terms of a more sensitive concentration range and a wide detection limit, or at least one.

Fig. 5 a) CV voltammogram of UA at 0.001–10  $\mu\text{M}$ ; (b) Histogram of UA concentration (0.001–10  $\mu\text{M}$ ) vs. anodic peak current; (c) plot of UA concentration (0.001–0.1  $\mu\text{M}$ ) vs. anodic peak current; (d) plot of UA concentration (1–10  $\mu\text{M}$ ) vs. anodic peak current.

Table 3. Comparison of the proposed uric acid sensor with literature reports

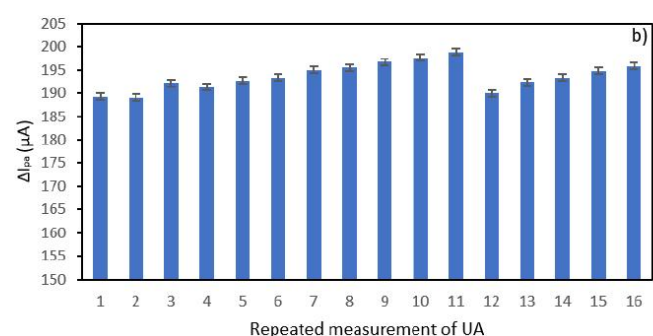
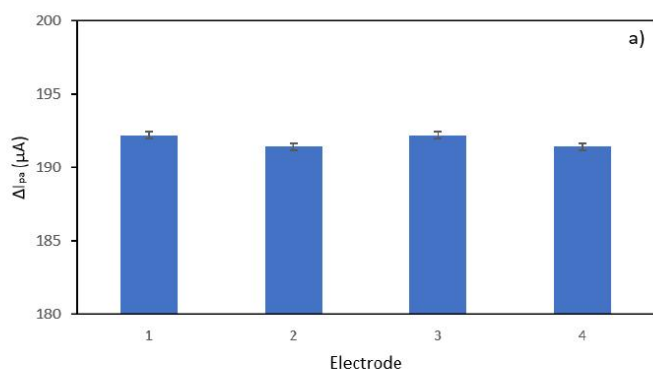
Electrode	pH	Linear Range	Detection limit	Ref
Hap-Esb/ZnONPs/ACE	8.0	10 to 10000 nM	15,79 nM	This work
HA/GCE	7.0	0.1 to 30.0 $\mu\text{M}$	0.142 $\mu\text{M}$	[8]
Graphene-modified carbon fiber	7.0	0.194 to 49.68 $\mu\text{M}$	0.132 $\mu\text{M}$	[61]
Pretreated-CPE	7.0	5 to 53.0 $\mu\text{M}$	5.0 $\mu\text{M}$	[62]
Carbon ionic liquid	6.8	2 to 220 $\mu\text{M}$	1.0 $\mu\text{M}$	[63]
Ce-HA/GCE	7.0	0.5 to 200 $\mu\text{M}$	0.39 $\mu\text{M}$	[13]
Poly(DPA)/SiO <sub>2</sub> @Fe <sub>3</sub> O <sub>4</sub> -CPE	7.0	1.2 to 8.2 $\mu\text{M}$	0.4 $\mu\text{M}$	[64]
Graphite-like pyrolytic carbon film	7.0	0.1 to 9.8 $\mu\text{M}$	0.03 $\mu\text{M}$	[65]
RGO-ZnO/GCE	6.0	1.0 to 70.0 $\mu\text{M}$	0.33 $\mu\text{M}$	[66]
Poly(bromocresol purple)/GCE	6.5	0.5 to 120 $\mu\text{M}$	0.20 $\mu\text{M}$	[67]
Nitrogen doped graphene	6.0	0.1 to 20.0 $\mu\text{M}$	0.045 $\mu\text{M}$	[68]
LaPO <sub>4</sub> /CPE	7.0	2.7 to 24.0 $\mu\text{M}$	0.09 $\mu\text{M}$	[69]
Graphene/size-selected Pt nanocomposites/GCE	7.0	0.05 to 11 $\mu\text{M}$	0.05 $\mu\text{M}$	[70]
N-rGO	7.0	1.0 to 30.0 $\mu\text{M}$	0.20 $\mu\text{M}$	[71]
PCN/MWCN	4.8	0.2 to 4.0 $\mu\text{M}$	0.139 $\mu\text{M}$	[72]
n-HA/CPE	7.0	0.068 to 50 $\mu\text{M}$	0.05 $\mu\text{M}$	[73]

#### Reproducibility, repeatability, and stability of the developed electrode

Reproducibility, repeatability, and stability all played important roles in evaluating the developed sensor's performance. Four equally prepared electrode were tested in 0.1  $\mu\text{M}$  UA solution to evaluate the reproducibility of Hap-Esb/ZnONPs/ACE by CV. The relative standard deviation (RSD) of the peak current response of UA was 0.24%. Next, the repeatability of our developed sensor was tested for 20/16 repetitive measurement. Before the repeating test, the developed sensor was washed with ultrapure water using the



CV for .. cycles to remove the analyte. The CV curve of the first measurement and the 20<sup>th</sup> measurement almost similar. And the calculation of RSD value result in 1.5% , indicating that the proposed



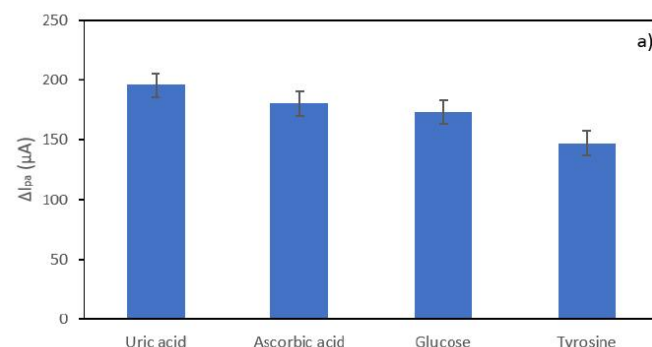
sensor has an excellent reproducibility and repeatability. Untuk stability?? (sebelumnya ditulis 3 bulan penyimpanan???) Datanya blm ada?)

Fig. 6 a) The peak current of 0.1 μM UA response on four different Hap-Esb/ZnONPs/ACE and b) the peak current of the repeatability measurement on an Hap-Esb/ZnONPs/ACE.

### Effect of potentially interfering species

In the aim to verify the selectivity of HAP-Esb/ZnONPs/ACE, the influence of several interfering species was evaluated. In this work the selectivity performance of Hap-Esb/ZnONPs/ACE was evaluated in the presence of glucose, ascorbic acid, and tyrosine. The interfering species were tested individually to detect any possibility of overlapping signals. The peak current responses of interfering were detected at potential of values -0.55 V, -0.44 V and -0.83 V (See Fig. Xa) with the peaks current response of 195.8 μA, 180.3 μA, 173.1 μA, and 147.2 μA (See Fig. Xb) for ascorbic acid, glucose, and tyrosine respectively. While, the UA response was detected at ... V at peak current response of ....., suggesting the selectivity of our modified sensor. Next the interference evaluation was further assessed by mixing the interferences at a ratio of 1:1. The CV voltammograms of UA in the presence of interfering are presented in Fig. Xa, whereas the comparative peak current response are presented in Fig. Xb. Notably, the presence of glucose and AA decreased the peak current response. In the pH optimization analysis, the pH value obviously influences the peak response of UA at Hap-Esb/ZnO/ACE. It seems the presence of AA increase the acidity then reducing the current response. Whereas the decrease

of UA peak current response in the presence of glucose might be due to the competition between glucose and urate ions to fill the



cavity of Hap-Esb [74], [75]. Given the difference of peak current responses are less than 10% (between 1-9.15%) [76], our proposed sensor shows a good selectivity.

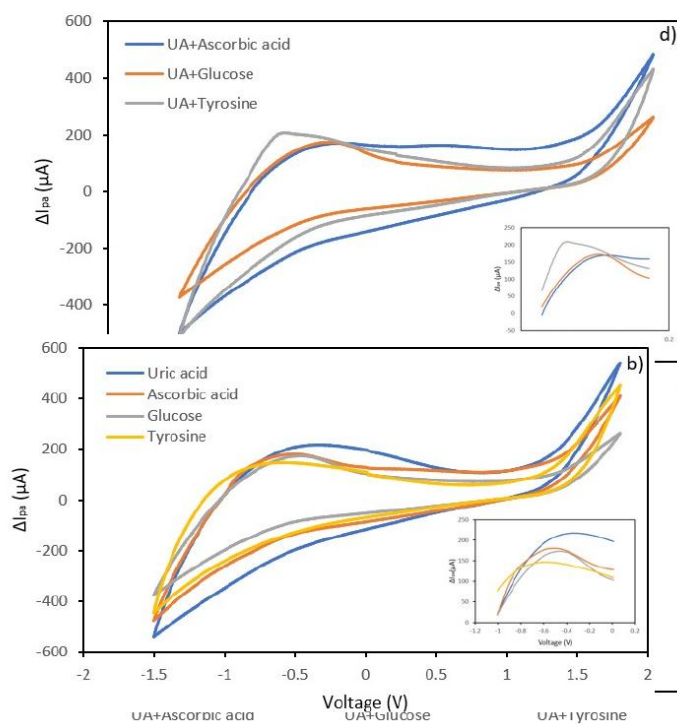


Fig. 7 a) Histogram of oxidation peak current of 0.1 μM interferent molecules on Hap-Esb/ZnONPs/ACE; b) Voltammogram of 0.1 μM interferent molecules on Hap-Esb/ZnONPs/ACE; c) histogram of oxidation peak current of 0.1 μM UA solution in the presence of interferences (0.1 μM) on Hap-Esb/ZnONPs/ACE; and d) Voltammogram of 0.1 μM UA solution in the presence of interferences (0.1 μM) on Hap/ZnONPs/ACE

## Conclusions

To find UA, electrochemical sensing based on Hap-Esb/ZnONPs/ACE was developed. The Hap-Esb/ZnONPs/ACE were prepared using a straightforward and efficient drop-casting method. Electrochemical experiments showed that the HAp powder-modified eggshell electrode worked well for UA detection at pH 7. It had a strong linear current response in the concentration range of 0.001  $\mu\text{M}$  to 10  $\mu\text{M}$ , with 0.001  $\mu\text{M}$  being the lowest concentration that could be detected. At the developed electrode, the UA had a LOD of 0.01579  $\mu\text{M}$  and a linear dynamic range of 0.001–10  $\mu\text{M}$ . After 16 more CV tests it was seen that the created electrode's repeatability performance was confirmed, as suggested by similar results. Most interestingly, when HAp from the eggshell was mixed with ZnONP, the current UA responded up to sixteen times better, showing better electrocatalytic activity. The validity of structural sensing efficacy has therefore been established.

## Conflicts of interest

There are no conflicts to declare.

## Acknowledgements

The authors thank Lingkungan dan Teknologi fiersih research group for guidance and this research is partly supported by the Direktorat Manajemen Talenta Deputi Sumber Daya Manusia IPTEK 2022 of fiadan Riset dan Inovasi Nasional with Contract No. 64/II/HK/2022. All this support is gratefully acknowledged.

## References

- [1] L. L. Jiang, X. Gong, M. Y. Ji, C. C. Wang, J. H. Wang, and M. H. Li, "Bioactive compounds from plant-based functional foods: A promising choice for the prevention and management of hyperuricemia," *Foods*, vol. 9, no. 8, 2020, doi: 10.3390/foods9080973.
- [2] M. A. Hediger, "Physiologie und biochemie der harnsäure," *Ther. Umschau*, vol. 61, no. 9, pp. 541–545, 2004, doi: 10.1024/0040-5930.61.9.541.
- [3] M. Kuwabara, "Hyperuricemia, Cardiovascular Disease, and Hypertension," *Pulse*, vol. 3, no. 3–4, pp. 242–252, 2015, doi: 10.1159/000443769.
- [4] W. L. Nyhan, "Lesch-Nyhan disease and related disorders of purine metabolism," *Tzu Chi Med. J.*, vol. 19, no. 3, pp. 105–108, 2007, doi: 10.1016/S1016-3190(10)60001-8.
- [5] A. Dehghan, M. Van Hoek, E. J. G. Sijbrands, A. Hofman, and J. C. M. Witteman, "High serum uric acid as a novel risk factor for type 2 diabetes," *Diabetes Care*, vol. 31, no. 2, pp. 361–362, 2008, doi: 10.2337/dc07-1276.
- [6] I. I. Hidayat, L. Hamijoyo, and M. A. Moeliono, "A survey on the clinical diagnosis and management of gout among general practitioners in fiandung," *Indones. J. Rheumatol.*, vol. 04, pp. 14–19, 2013.
- [7] X. L. Jin Jun Luo, "A Double-edged Sword: Uric Acid and Neurological Disorders," *Brain Disord. Ther.*, vol. 02, no. 02, pp. 109–111, 2013, doi: 10.4172/2168-975x.1000109.
- [8] P. Kanchana and C. Sekar, "EDTA assisted synthesis of hydroxyapatite nanoparticles for electrochemical sensing of uric acid," *Mater. Sci. Eng. C*, 2014, doi: 10.1016/j.msec.2014.05.072.
- [9] V. A. Online and S. Radhakrishnan, "RSC Advances," 2015, doi: 10.1039/C5RA06763D.
- [10] A. S. Sundarraj, S. Justin, S. Joseph, V. S. Rajadurai, and P. Wilson, "l-arginine directed and ultrasonically aided growth of nanocrystalline hydroxyapatite particles with tunable morphology," *Colloids Surfaces A Physicochem. Eng. Asp.*, 2017, doi: 10.1016/j.colsurfa.2017.11.012.
- [11] M. Aizawa, A. E. Porter, S. M. Fiest, and W. Fionfield, "Ultrastructural observation of single-crystal apatite fibres," vol. 26, pp. 3427–3433, 2005, doi: 10.1016/j.biomaterials.2004.09.044.
- [12] K. Sugo and T. Okuyama, "Ac c ep te d us cr t," vol. 6395, no. September, 2017, doi: 10.1080/01496395.2017.1380047.
- [13] P. Kanchana, M. Navaneethan, and C. Sekar, "Materials Science & Engineering fi Fabrication of Ce doped hydroxyapatite nanoparticles based non-enzymatic electrochemical sensor for the simultaneous determination of norepinephrine , uric acid and tyrosine," vol. 226, no. June, pp. 132–140, 2017, doi: 10.1016/j.mseb.2017.09.015.
- [14] E. S. P. fi. V, "Review Hydroxyapatite as a liquid chromatographic packing," vol. 544, pp. 147–184, 1991.
- [15] E. S. P. fi. V, "liquid chromatography," vol. 515, pp. 125–148, 1990.
- [16] Y. Li *et al.*, "Sensors and Actuators fi : Chemical Simultaneous determination of ultra-trace lead and cadmium at a hydroxyapatite-modified carbon ionic liquid electrode by square-wave stripping voltammetry," vol. 139, pp. 604–610, 2009, doi: 10.1016/j.snb.2009.03.045.
- [17] J. M. Chem, "Conversion of egg-shell to hydroxyapatite for highly sensitive detection of endocrine disruptor bisphenol A †," pp. 14428–14431, 2011, doi: 10.1039/c1jm12544c.
- [18] fi. Wang, J. Zhang, Z. Pan, X. Tao, and H. Wang, "fiiosensors and fiioelectronics A novel hydrogen peroxide sensor based on the direct electron transfer of horseradish peroxidase immobilized on silica – hydroxyapatite hybrid film," vol. 24, pp. 1141–1145, 2009, doi: 10.1016/j.bios.2008.06.053.

- [19] P. S. L. Pandharipande, "Synthesis of Hydroxyapatite from egg shell and preparation of bone like fiio-composites using it," *Int. J. Adv. Inf. Sci. Technol.*, vol. 52, no. 52, pp. 36–47, 2016, doi: 10.15693/ijaist/2016.v5i8.
- [20] C. X. Wang, M. Wang, and X. Zhou, "Nucleation and growth of apatite on chemically treated titanium alloy: An electrochemical impedance spectroscopy study," *Biomaterials*, vol. 24, no. 18, pp. 3069–3077, 2003, doi: 10.1016/S0142-9612(03)00154-6.
- [21] Z. Zyman, J. Weng, X. Liut, X. Lit, and X. Zhang, "Phase and structural changes in hydroxyapatite coatings under heat treatment," vol. 15, no. 2, 1994.
- [22] K. Ozeki, J. M. Janurudin, H. Aoki, and Y. Fukui, "Photocatalytic hydroxyapatite/titanium dioxide multilayer thin film deposited onto glass using an rf magnetron sputtering technique," *Appl. Surf. Sci.*, vol. 253, no. 7, pp. 3397–3401, 2007, doi: 10.1016/j.apsusc.2006.07.030.
- [23] A. Manuscript, "Materials Chemistry A," 2016, doi: 10.1039/C6TA01528J.
- [24] A. Manuscript, "Materials Chemistry fi," 2014, doi: 10.1039/C4TF01651C.
- [25] D. Lakshmi, M. J. Whitcombe, F. Davis, S. Sharma, and fi. Prasad, "Electrochemical Detection of Uric Acid in Mixed and Clinical Samples : A Review," pp. 305–320, 2011, doi: 10.1002/elan.201000525.
- [26] K. Shi and K. Shiu, "Determination of Uric Acid at Electrochemically Activated Glassy Carbon Electrode," pp. 2–8, 2001.
- [27] fi. Uslu, "The Analytical Applications of Square Wave Voltammetry on Pharmaceutical Analysis," *Open Chem. Biomed. Methods J.*, vol. 3, no. 1, pp. 56–73, 2011, doi: 10.2174/1875038901003010056.
- [28] T. Sen, S. Mishra, S. S. Sonawane, and N. G. Shimpi, "Polyaniline / Zinc Oxide Nanocomposite as Room-Temperature Sensing Layer for Methane," pp. 1–8, 2017, doi: 10.1002/pen.24740.
- [29] M. R. Ganjali, F. G. Nejad, and H. feitollahi, "Highly Sensitive Voltammetric Sensor for Determination of Ascorbic Acid Using Graphite Screen Printed Electrode Modified with ZnO / Al<sub>2</sub>O<sub>3</sub> Nanocomposite," vol. 12, p. 3240, 2017, doi: 10.20964/2017.04.07.
- [30] V. Singh, M. Hojamberdiev, and M. Kumar, "Enhanced sensing performance of ZnO nanostructures-based gas sensors : A review," *Energy Reports*, no. xxxx, 2019, doi: 10.1016/j.egy.2019.08.070.
- [31] M. Ghaedi *et al.*, "Preparation of Iodide Selective Carbon Paste Electrode with Modified Carbon Nanotubes by Potentiometric Method and Effect of CuS-NPs on Its Response," *Electroanalysis*, vol. 27, no. 6, pp. 1516–1522, 2015, doi: 10.1002/elan.201400686.
- [32] M. Luqman, M. Napi, S. M. Sultan, and R. Ismail, "Electrochemical-fiated fiiosensors on Di ff erent Zinc," pp. 1–34, 2019.
- [33] Z. Wang, H. Li, F. Tang, J. Ma, and X. Zhou, "A Facile Approach for the Preparation of Nano-size Zinc Oxide in Water / Glycerol with Extremely Concentrated Zinc Sources," pp. 1–9, 2018.
- [34] T. Kokab *et al.*, "Simultaneous Femtomolar Detection of Paracetamol , Diclofenac , and Orphenadrine Using a Carbon Nanotube / Zinc Oxide Nanoparticle-fiated Electrochemical Sensor," 2021, doi: 10.1021/acsnm.1c00310.
- [35] P. Louka and C. fi. Anders, "A role of ZnO nanoparticle electrostatic properties in cancer cell cytotoxicity," pp. 29–45, 2016.
- [36] "ZnO Nanoparticle Modified Carbon Paste Electrode as a Sensor for Electrochemical Determination of Tert-fiutylhydroquinone in Food Samples.pdf."
- [37] S. A. Shahamirifard and M. Ghaedi, "A new electrochemical sensor for simultaneous determination of arbutin and vitamin C based on hydroxyapatite-ZnO-Pd nanoparticles modified carbon paste electrode," *Biosens. Bioelectron.*, p. 111474, 2019, doi: 10.1016/j.bios.2019.111474.
- [38] R. Sadeghi, H. Karimi-maleh, and A. fiahari, "Physics and Chemistry of Liquids : An A novel biosensor based on ZnO bromide ionic liquid-modified carbon paste electrode for square-wave voltammetric determination of epinephrine," no. September, pp. 37–41, 2013, doi: 10.1080/00319104.2013.782547.
- [39] fi. Gu, C. Xu, C. Yang, S. Liu, and M. Wang, "fiiosensors and fiioelectronics ZnO quantum dot labeled immunosensor for carbohydrate antigen 19-9," *Biosens. Bioelectron.*, vol. 26, no. 5, pp. 2720–2723, 2011, doi: 10.1016/j.bios.2010.09.031.
- [40] H. Y. Zhao, H. M. Zhou, J. X. Zhang, W. Zheng, and Y. F. Zheng, "fiiosensors and fiioelectronics Carbon nanotube – hydroxyapatite nanocomposite : A novel platform for glucose / O<sub>2</sub> biofuel cell," vol. 25, pp. 463–468, 2009, doi: 10.1016/j.bios.2009.08.005.
- [41] M. I. Sabela, "SC," *JEAC*, 2016, doi: 10.1016/j.jelechem.2016.05.021.
- [42] "Version of Record: <https://www.sciencedirect.com/science/article/pii/S2352710219302086>," 2019.
- [43] F. S. Murakami, P. O. Rodrigues, C. Maria, T. De Campos, M. Antônio, and S. Silva, "Physicochemical study of CaCO<sub>3</sub> from egg shells," vol. 27, no. 3, pp. 658–662, 2007.

- [44] F. Hilbrig and R. Freitag, "Hydroxyapatite in fioprocessing," 2012.
- [45] A. Afshar, M. Ghorbani, N. Ehsani, M. R. Saeri, and C. C. Sorrell, "Some important factors in the wet precipitation process of hydroxyapatite," vol. 24, no. 03, pp. 197–202, 2003, doi: 10.1016/S0261-3069(03)00003-7.
- [46] fi. Koch, "X-ray diffraction studies on plasma-sprayed calcium phosphate-coated implants," vol. 24, pp. 655–667, 1990.
- [47] J. Weng, X. Liu, X. Zhang, Z. Ma, X. Ji, and Z. Zyman, "Further studies on the plasma-sprayed amorphous phase in hydroxyapatite coatings and its deamorphization," pp. 578–582, 1993.
- [48] K. A. Gross and C. C. fierndt, "Thermal processing of hydroxyapatite for coating production," 1997.
- [49] N. Hydrogels, N. fiouropoulos, A. Stampolakis, and D. E. Mouzakis, "Dynamic Mechanical Properties of Calcium Alginate-Hydroxyapatite Dynamic Mechanical Properties of Calcium Alginate-Hydroxyapatite Nanocomposite Hydrogels," no. April 2017, pp. 1–5, 2010, doi: 10.1166/sam.2010.1092.
- [50] M. Tagaya, T. Ikoma, and N. Hanagata, "Reusable hydroxyapatite nanocrystal sensors for protein adsorption," vol. 045002, doi: 10.1088/1468-6996/11/4/045002.
- [51] M. A. M. Ikram, M. I. A. Ul, and H. M. Avais, "Green synthesis and evaluation of n - type ZnO nanoparticles doped with plant extract for use as alternative antibacterials," *Appl. Nanosci.*, 2020, doi: 10.1007/s13204-020-01451-6.
- [52] D. Jain *et al.*, "properties i v o r l a n o i v o l," 2020, doi: 10.3389/fchem.2020.00778.
- [53] Z. M. Al-asady, A. H. Al-hamdani, and M. A. Hussein, "Study the optical and morphology properties of zinc oxide nanoparticles Study the Optical and Morphology Properties of Zinc Oxide Nanoparticles," vol. 020061, no. March, 2020.
- [54] A. fi. Lavand and Y. S. Malghe, "Synthesis, characterization and visible light photocatalytic activity of nitrogen-doped zinc oxide nanospheres," *Integr. Med. Res.*, pp. 2–7, 2015, doi: 10.1016/j.jascer.2015.06.002.
- [55] R. Sabry, M. Fikry, O. S. Ahmed, and A. R. N. Zekri, "Laser-Induced Synthesis of Pure Zinc Oxide Nanoflakes Laser-Induced Synthesis of Pure Zinc Oxide Nanoflakes," 2020, doi: 10.1088/1742-6596/1472/1/012005.
- [56] L. Khalafi, *Cyclic voltammetry*, no. Cv. 2017.
- [57] N. Thakur, D. Mandal, and T. C. Nagaiah, "Highly sensitive non-enzymatic electrochemical glucose sensor surpassing water oxidation interference," 2021.
- [58] A. Manuscript, "Materials Chemistry A," 2014, doi: 10.1039/b000000x.
- [59] G. fiharath, A. J. Kumar, K. Karthick, D. Mangalaraj, and C. Viswanathan, "RSC Advances mesoporous hydroxyapatite nanostructures and their morphology dependent Pb ( II ) removal from waste water," *RSC Adv.*, vol. 4, pp. 37446–37457, 2014, doi: 10.1039/C4RA06929C.
- [60] G. Viscusi, G. fiarra, and G. Gorrasi, "Modification of hemp fibers through alkaline attack assisted by mechanical milling: effect of processing time on the morphology of the system," *Cellulose*, vol. 27, no. 15, pp. 8653–8665, 2020, doi: 10.1007/s10570-020-03406-0.
- [61] J. Du *et al.*, "Colloids and Surfaces A : Physicochemical and Engineering Aspects Nonenzymatic uric acid electrochemical sensor based on graphene-modified carbon fiber electrode," *Colloids Surfaces A Physicochem. Eng. Asp.*, vol. 419, pp. 94–99, 2013, doi: 10.1016/j.colsurfa.2012.11.060.
- [62] H. Umveraty, "AN IMPROVED VOLTAMMETRIC METHOD FOR THE DETERMINATION OF TRACE AMOUNTS OF URIC ACID WITH ELECTROCHEMICALLY PRETREATED CARFION PASTE ELECTRODES," vol. 41, no. 3, pp. 407–413.
- [63] A. Safavi, N. Maleki, O. Moradlou, and F. Tajabadi, "Simultaneous determination of dopamine , ascorbic acid , and uric acid using carbon ionic liquid electrode," vol. 359, pp. 224–229, 2006, doi: 10.1016/j.ab.2006.09.008.
- [64] Y. V. M. Reddy, fi. Sravani, S. Agarwal, V. K. Guptha, and G. Madhavi, "US," *J. Electroanal. Chem.*, p. #pagerange#, 2018, doi: 10.1016/j.jelechem.2018.04.059.
- [65] M. Hadi and A. Rouhollahi, "Analytica Chimica Acta Simultaneous electrochemical sensing of ascorbic acid , dopamine and uric acid at anodized nanocrystalline graphite-like pyrolytic carbon film electrode," *Anal. Chim. Acta*, vol. 721, pp. 55–60, 2012, doi: 10.1016/j.aca.2012.01.051.
- [66] X. Zhang, Y. Zhang, and L. Ma, "Sensors and Actuators fi : Chemical One-pot facile fabrication of graphene-zinc oxide composite and its enhanced sensitivity for simultaneous electrochemical detection of ascorbic acid , dopamine and uric acid," *Sensors Actuators B. Chem.*, vol. 227, pp. 488–496, 2016, doi: 10.1016/j.snb.2015.12.073.
- [67] Y. Wang and L. Tong, "Sensors and Actuators fi : Chemical Electrochemical sensor for simultaneous determination of uric acid , xanthine and hypoxanthine based on poly ( bromocresol purple ) modified glassy carbon electrode," *Sensors Actuators B. Chem.*, vol. 150, no. 1, pp. 43–49, 2010, doi: 10.1016/j.snb.2010.07.044.
- [68] Z. Sheng, X. Zheng, J. Xu, W. fiao, F. Wang, and X. Xia, "fiiosensors and fioelectronics Electrochemical sensor based on nitrogen doped graphene : Simultaneous determination of ascorbic acid , dopamine and uric acid,"



- Biosens. Bioelectron.*, vol. 34, no. 1, pp. 125–131, 2012, doi: 10.1016/j.bios.2012.01.030.
- [69] Y. Zhou, H. Zhang, H. Xie, fi. Chen, L. Zhang, and X. Zheng, “Electrochimica Acta A novel sensor based on LaPO<sub>4</sub> nanowires modified electrode for sensitive simultaneous determination of dopamine and uric acid,” vol. 75, pp. 360–365, 2012.
- [70] C. Sun, H. Lee, J. Yang, and C. Wu, “fiosensors and fioelectronics The simultaneous electrochemical detection of ascorbic acid , dopamine , and uric acid using graphene / size-selected Pt nanocomposites,” *Biosens. Bioelectron.*, vol. 26, no. 8, pp. 3450–3455, 2011, doi: 10.1016/j.bios.2011.01.023.
- [71] H. Zhang and S. Liu, “Electrochemical biosensors based on nitrogen-doped reduced graphene oxide for the simultaneous detection of ascorbic acid, dopamine and uric acid,” *J. Alloys Compd.*, p. 155873, 2020, doi: 10.1016/j.jallcom.2020.155873.
- [72] J. Lv *et al.*, “A novel electrochemical sensor for uric acid detection based on PCN / MWCNT,” 2019.
- [73] E. Iyyappan, S. J. S. J., P. Wilson, and P. Arumugam, “Nanoscale Hydroxyapatite for Electrochemical Sensing of Uric Acid : Roles of Mesopore Volume and Surface Acidity,” 2020, doi: 10.1021/acsanm.0c01322.
- [74] R. A. Tama, “Cyclic voltammetry of glucose , uric acid , and cholesterol using gold electrode Cyclic Voltammetry of Glucose , Uric Acid , and Cholesterol Using Gold Electrode,” vol. 030037, no. April, 2020.
- [75] H. Darmokoesoemo, N. Widayanti, Y. Kadmi, M. Khasanah, H. S. Kusuma, and H. Elmsellem, “Development of Carbon Paste Electrodes Modified by Molecularly Imprinted Polymer as Potentiometry Sensor of Uric Acid,” *Results Phys.*, 2017, doi: 10.1016/j.rinp.2017.05.013.
- [76] fi. Pandiripalli, “REPEATABILITY AND REPRODUCIBILITY STUDIES: A COMPARISON OF TECHNIQUES,” no. December, 2010.